Supplementary materials

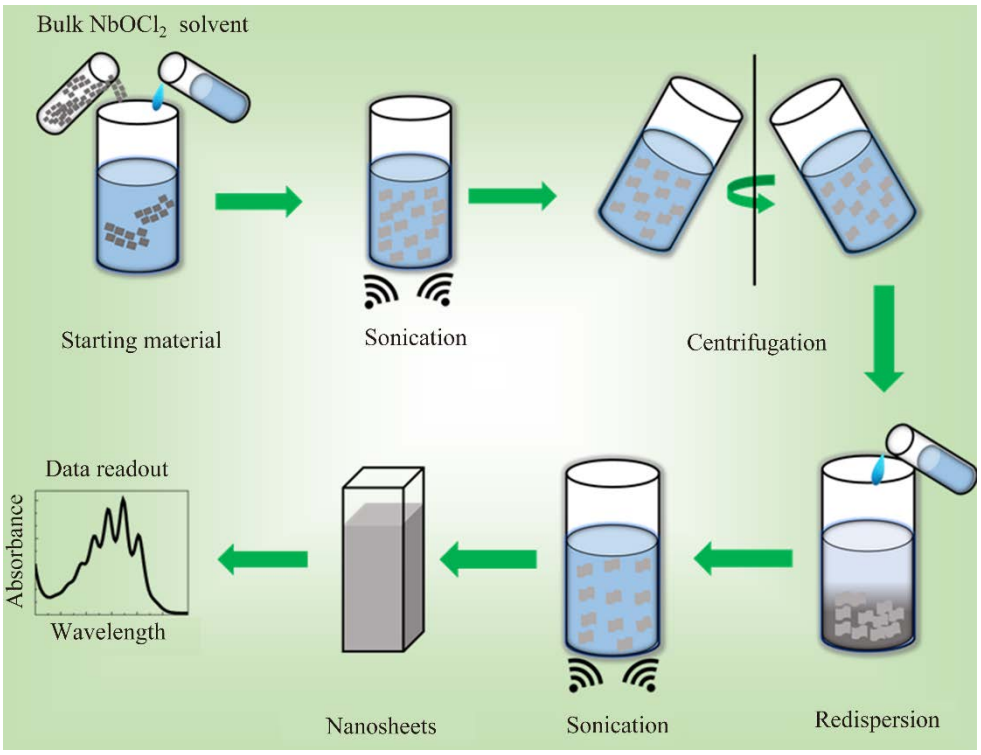

Figure S1 Schematic representation of the production of $NbOCl_2$ nanosheets by the LPE process

The liquid phase exfoliation (LPE) procedure comprises essential stages. Initially, bulk $NbOCl_2$ is dispersed in a compatible solvent and then treated with an ultrasound sonication process to exfoliate the nanoparticles. The resulting nanosheets are subsequently centrifugated to segregate any residual material, consenting for precise control over the nanosheet size. After centrifugation, the nanosheets are redispersed in a fresh solvent (bath sonication for several minutes) to create a homogeneous solution for comprehensive analysis using UV-Vis spectrometry.

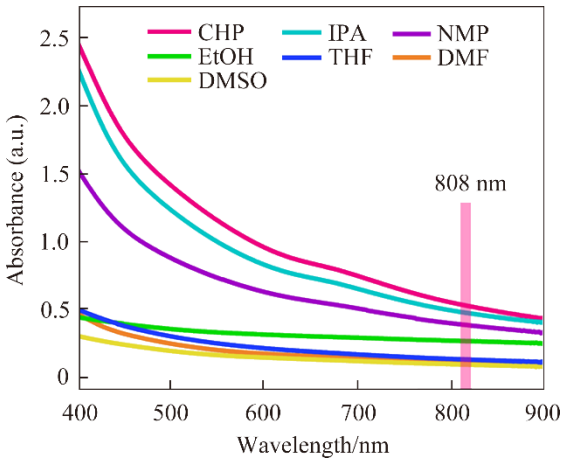

Figure S2 The optical absorbance spectra of $NbOCl_2$ distribution in seven solvents revealing significant absorption from UV to the infrared range

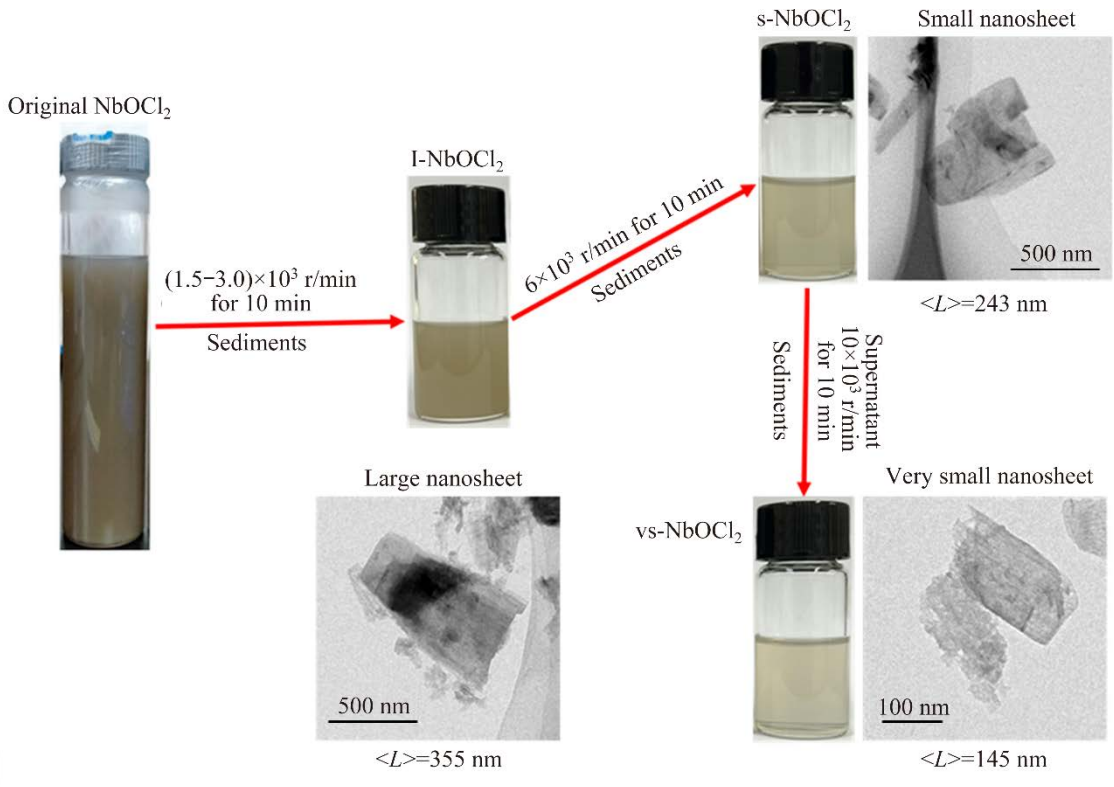

Figure S3 Schematic illustration of the size selection process to acquire large, small, and very small $NbOCl_2$ nanosheets utilized throughout the main manuscript

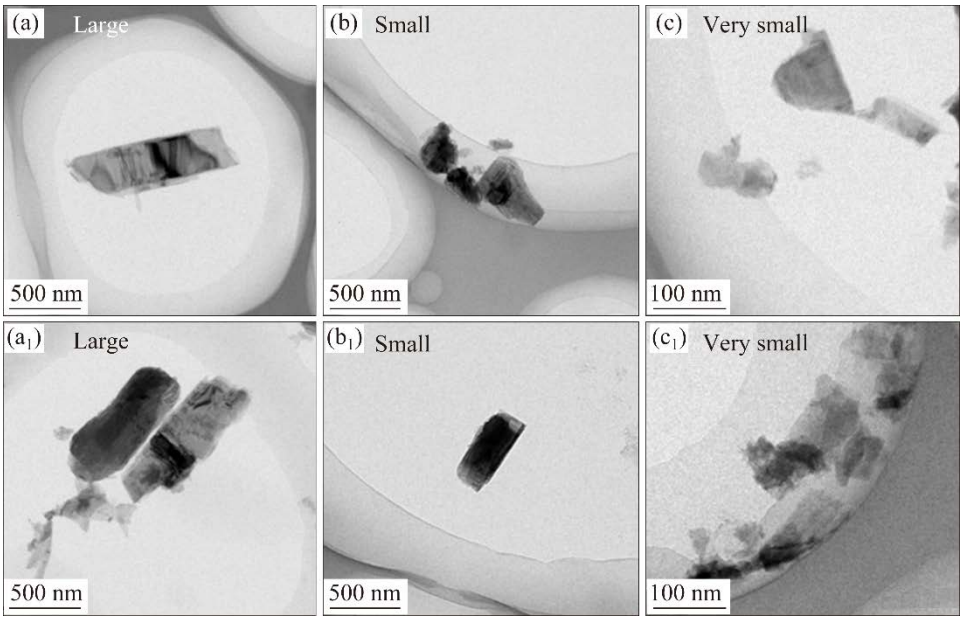

Figure S4 Low-resolution TEM images with varying sizes of (a, a_1) large, (b, b_1) small, and (c, c_1) very small $NbOCl_2$ nanosheets dispersed in IPA

Calculation of the photothermal conversion efficiency

The photothermal conversion efficiency of $NbOCl_2$ was evaluated by exposing a sample in an NMP dispersion to continuous laser irradiation. Temperature changes were monitored over time until reaching a peak temperature, at which point the laser was deactivated. The subsequent cooling process was observed until the temperature returned to room level. The photothermal conversion efficiency (η) was then calculated using a

prescribed equation based on the recorded temperature data.

$$\sum_i m_i C_{p,i} \frac{\mathrm{d}T}{\mathrm{d}t} = Q_{\mathrm{NbOCl_2}} + Q_{\mathrm{Dis}} - Q_{\mathrm{surr}} \tag{S1}$$

where T represents the system surface temperature; m_i is the mass and the heat capacity of the system is represented by $C_{p,i}$; $Q_{\mathrm{NbOCl_2}}$ is the energy input of $NbOCl_2$ nanosheets; Q_{Dis} is the baseline energy input of the sample cell, represents the heat dissipation from the sample cell due to light absorption, and is measured independently to be $Q_{\mathrm{Dis}}=3.40\times10^{-3}\,I$ (in unit of mW) using a sample cell containing pure NMP; Q_{surr} is the heat dissipated into the surrounding air and is a temperature-dependent parameter linearly related to thermal energy output. The NIR laser-induced source term, $Q_{\mathrm{NbOCl_2}}$, describes the heat dissipated by electron-phonon relaxation of the plasmon on the $NbOCl_2$ nanosheets' surface under 808 nm laser irradiation.

$$Q_{\mathrm{NbOCl_2}} = I(1-10^{-A\lambda}) \tag{S2}$$

where I is the incident energy of the NIR laser (mW), $A\lambda$ is the absorbance of the $NbOCl_2$ nanosheets at 808 nm, and η is the photothermal efficiency of converting NIR laser energy to heat energy.

$$Q_{\mathrm{surr}}=hS(T_{\mathrm{max}}-T_{\mathrm{surr}}) \tag{S3}$$

where h indicates the heat-transfer coefficient; S is the container's surface area; T_{max} is the maximum system temperature; T_{surr} represents surrounding temperature, respectively.

$$\eta = \frac{hS(T_{\mathrm{max}} - T_{\mathrm{surr}}) - Q_{\mathrm{Dis}}}{I(1-10^{-A\lambda})} \tag{S4}$$

The absorbance of $NbOCl_2$ nanosheets is signified as $A\lambda$. Thus, only the hS remains unidentified for the calculation of η. To calculate hS, a dimensionless driving force temperature, denoted as θ, is introduced in the following manner.:

$$\theta = \frac{T - T_{\mathrm{surr}}}{T_{\mathrm{max}} - T_{\mathrm{surr}}} \tag{S5}$$

Here T represents the temperature of the $NbOCl_2$ solution, T_{max} is the maximum system temperature, and T_{surr} is surrounding temperature.

$$\tau_{\mathrm{s}} = \frac{\Sigma_i m_i c_{p,i}}{hS} \tag{S6}$$

For a time constant τ_{s} of the sample system, thus

$$\frac{\mathrm{d}\theta}{\mathrm{d}t} = \frac{1}{\tau_{\mathrm{s}}}\left(\frac{Q_{\mathrm{NbOCl_2}} + Q_{\mathrm{Dis}}}{hS\Delta T_{\mathrm{max}}} - \theta\right) \tag{S7}$$

When the laser is turned off, $Q_{\mathrm{NbOCl_2}}+Q_{\mathrm{Dis}}=0$, $\mathrm{d}\theta/\mathrm{d}t=-/\tau_{\mathrm{s}}$, $t=-\tau_{\mathrm{s}}\ln\theta$. So, hS could be calculated from the slope of cooling time *vs* $\ln\theta$. The time constant (τ_{s}) of heat transfer from $NbOCl_2$ for 808 nm was determined to be 53.15 s at 1.25 W/cm^2. The $T_{\mathrm{max}}-T_{\mathrm{surr}}$ of $NbOCl_2$ was 12.2 °C for 808 nm laser irradiation. Therefore, the photothermal conversion efficiency (η) of $NbOCl_2$ was calculated to be 31.37% at 808 nm under different power density.

Table S1 Summary of the photothermal conversion efficiency of $NbOCl_2$ in this work compared with other photothermal agents from some previous reports

Material	Absorbance coefficient/($L \cdot g^{-1} \cdot cm^{-1}$)	Photothermal conservation efficiency, η/%	Wavelength/nm	References
$NbOCl_2$	30.26	31.37	808	This work
IR1048-MZ	20.2	20.2	808	[1]
Au NRs	13.9	21	808	[2]
MoS_2	29.2	24.37	808	[3]
WS_2	23.8	44.3	808	[4]
Nb_2C	37.6	36.5	808	[5]
SnS	16.2	24	808	[6]
BP QDs	14.8	28.4	808	[7]
Ti_3C_2	25.2	30.6	808	[8]
Ta_2NiS_5	25.6	35	808	[9]

References

[1] MENG Xiao-qing, ZHANG Jia-li, SUN Zhi-hong, et al. Hypoxia-triggered single molecule probe for high-contrast NIR II/PA tumor imaging and robust photothermal therapy [J]. Theranostics, 2018, 8(21): 6025−6034. DOI: 10.7150/thno.26607.

[2] ZENG Jie, GOLDFELD D, XIA You-nan. A plasmon-assisted optofluidic (PAOF) system for measuring the photothermal conversion efficiencies of gold nanostructures and controlling an electrical switch [J]. Angewandte Chemie International Edition, 2013, 52(15): 4169−4173. DOI: 10.1002/anie.201210359.

[3] LIU Teng, WANG Chao, GU Xing, et al. Drug delivery with PEGylated MoS_2 nano-sheets for combined photothermal and chemotherapy of cancer [J]. Advanced Materials, 2014, 26(21): 3433−3440. DOI: 10.1002/adma.201305256.

[4] YONG Yuan, CHENG Xia-ju, BAO Tao, et al. Tungsten sulfide quantum dots as multifunctional nanotheranostics for *in vivo* dual-modal image-guided photothermal/radiotherapy synergistic therapy [J]. ACS Nano, 2015, 9(12): 12451−12463. DOI: 10.1021/acsnano.5b05825.

[5] LIN Han, GAO Shan-shan, DAI Chen, et al. A two-dimensional biodegradable niobium carbide (MXene) for photothermal tumor eradication in NIR-I and NIR-II biowindows [J]. Journal of the American Chemical Society, 2017, 139(45): 16235−16247. DOI: 10.1021/jacs.7b07818.

[6] REN Qi-long, LI Bo, PENG Zhi-you, et al. SnS nanosheets for efficient photothermal therapy [J]. New Journal of Chemistry, 2016, 40(5): 4464−4467. DOI: 10.1039/C5NJ03263F.

[7] SUN Zheng-bo, XIE Han-han, TANG Si-ying, et al. Ultrasmall black phosphorus quantum dots: Synthesis and use as photothermal agents [J]. Angewandte Chemie (International Ed), 2015, 54(39): 11526−11530. DOI: 10.1002/anie.201506154.

[8] XUAN Jin-nan, WANG Zhi-qiang, CHEN Yu-yan, et al. Organic-base-driven intercalation and delamination for the production of functionalized titanium carbide nanosheets with superior photothermal therapeutic performance [J]. Angewandte Chemie (International Ed), 2016, 55(47): 14569−14574. DOI: 10.1002/anie.201606643.

[9] ZHU Hou-juan, LAI Zhuang-chai, FANG Yuan, et al. Ternary chalcogenide nanosheets with ultrahigh photothermal conversion efficiency for photoacoustic theranostics [J]. Small, 2017, 13(16). DOI: 10.1002/smll.201604139.